

# Influence of electron beam welding parameters on microstructure and Charpy impact properties of boron-added modified 9Cr-1Mo steel weld

C. R. Das<sup>1</sup> · A. K. Bhaduri<sup>1</sup> · S. Raju<sup>1</sup> · R. Balakrishnan<sup>1</sup> · S. Mahadevan<sup>1</sup> · S. K. Albert<sup>1</sup> · P. Mastanaiah<sup>2</sup>

Received: 3 January 2016 / Accepted: 21 June 2016 / Published online: 19 July 2016  
© International Institute of Welding 2016

**Abstract** The effect of electron beam welding parameters on microstructure and ductile-to-brittle transition temperature (DBTT) of a boron-added modified 9Cr-1Mo steel weld is presented in this paper. Compared to the base metal, for the weld, the upper shelf energy is lower and the DBTT is significantly lower. While the influence of welding parameters on the upper shelf energy of the weld is insignificant, its influence on the transition region and the lower shelf region is quite significant due to the presence of delta-ferrite in the weld. High welding speed reduces the time available for transformation of delta-ferrite to austenite and results in retention of delta-ferrite in weld. Lower welding speed promotes completion of delta-ferrite to austenite transformation as cooling rate reduces which improves lower shelf energy.

**Keywords** EB welding · Microstructure · Mechanical properties · B additions · High alloy Cr Mo steels · Transformation temperature · Welded joint

## 1 Introduction

Modified 9Cr-1Mo (P91) steel is commonly used in power plants and petrochemical industries at temperatures up to

600 °C due to its superior thermophysical properties and adequate mechanical properties compared to austenitic stainless steels. This material is usually used in the normalized and tempered condition, in which the microstructure consists of tempered lath martensite with precipitates decorating the lath, block, packet, and prior austenite grain boundaries [1]. Improved creep strength of P91 steel over the plane 9Cr-1Mo (P9) steel is due to the presence of MX type of carbides, nitrides, and carbonitrides [2]. Addition of boron in P91 steel with controlled nitrogen is reported to significantly improve its creep strength [3]. However, in the boron-added P91 (P91B) steel, to ensure the beneficial effect of boron addition, the formation of the brittle boron nitride (BN) phase needs to be avoided by significantly reducing the nitrogen content in the P91B steel compared to that in the boron-free P91 steel. Also, increasing the normalizing temperature for the P91B steel improves the creep strength of the base metal and also its weld joint made using boron-free modified 9Cr-1Mo steel welding consumable [3]. The use of boron-free modified 9Cr-1Mo steel weld to join the P91B base metal makes the weld microstructure relatively unstable resulting in the formation of creep cavities in the weld metal during creep testing. The use of ENiCrFe-3 (Inconel 182) filler wire for welding boron-containing 9 Cr-3 W-3 Co-V-Nb steel showed significant improvement in the creep strength of its weld joint compared to weld joints of P91 steel [4]. Different types of welding filler wires to achieve matching, under-matching, and over-matching of strength, viz. P91, E911, and P92, for joining boron-containing 9 Cr-3 W-3 Co-V-Nb steel with controlled nitrogen have shown improvement in the creep strength of the weld joints [5]. It is, therefore, evident that boron-containing P91 welding consumable is essential to provide microstructural stability to the weld metal as in P91B base metal used. Though the P91-type materials are designed for high temperature application, its ambient temperature toughness is equally

---

Recommended for publication by Commission IX - Behaviour of Metals Subjected to Welding

---

✉ A. K. Bhaduri  
bhaduri@igcar.gov.in

<sup>1</sup> Indira Gandhi Centre for Atomic Research, Kalpakkam 603102, India

<sup>2</sup> Defence Research & Development Laboratory, Hyderabad, India

important as the fabricated component made of this material may have to be qualified by hydro-testing.

In the absence of boron-containing welding consumable to weld the P91B material, electron beam (EB) welding of this material without filler addition has been carried out in this work to ensure that the weld metal has matching composition to that of the base metal. The high-energy density EB welding process provides for deep penetration and large depth-to-width ratio of the weld bead, reduced width of the heat affected zone (HAZ) and distortion. As in the EB welding process, the energy is transferred through the keyhole along the thickness direction, in high-chromium ferritic steels, welding speed has significant influence on liquid to solid and high-temperature solid-state transformation. Hence, the effect of EB welding parameters on the phase transformations, microstructural evolution, and ductile-to-brittle transition temperature (DBTT) has been studied.

## 2 Experimental

Plates of size  $250 \times 150 \times 12 \text{ mm}^3$  of a P91B steel, with chemical composition as given in Table 1, in the normalized and tempered condition, were used for the preparation of EB welded joints. Prior to welding, a defocused electron beam was used for preheating the plates. The welding parameters used for welding the three test weld pads are given in Table 2. All weld joints were inspected by radiography examination and were found to be free from defects. Subsequently, the weld joints were subjected to post-weld heat treatment (PWHT) at  $760 \text{ }^\circ\text{C}$  for 3 h [6].

Differential scanning calorimetry (DSC) study was performed in order to understand the phase transformation occurring during heating and cooling. Thermodynamic equilibrium calculations were carried out using ThermoCalc software with Tcf6 data bases. Microstructures of weld were observed in a scanning electron microscope (SEM) in the as-welded and PWHT conditions after etching with Villella's reagent. Charpy V-notch (CVN) impact specimens, with the notch oriented in the welding direction, from the three weld pads and the P91B base material were prepared. Full-size CVN specimens were prepared from the W1 weld pad and the P91B base plate, and half-size CVN specimens were prepared from W2 and W3 weld pads in PWHT conditions. The impact tests were carried out at ambient and sub-zero temperatures to evaluate the DBTT. SEM fractography of the impact tested specimens

were also carried out. Conversion factor of 2 is used for converting half size value into full size value. Two specimens were used from each condition.

## 3 Results and discussion

### 3.1 Microstructure

The P91B steel EB weld metals after PWHT have a microstructure consisting of lath martensite with precipitates decorating the lath boundaries (Fig. 1). Significantly, more polygonal delta-ferrite is observed in W1 weld metal (Fig. 1a) than in W2 weld metal (Fig. 1b). Delta-ferrite is not observed in W3 weld metal (Fig. 1c). Area fraction of delta-ferrite in W1 and W2 weld metal is estimated to be 0.015 and 0.05. As delta-ferrite was not measurable for W3 weld, it was not estimated. The variations in delta-ferrite content in the weld metals are due to the variation in heat input that causes variation in the time available for the  $\delta \rightarrow \gamma$  phase transformation. The SEM micrograph of the W1 weld metal in the as-welded condition reveals the presence of significant amount of polygonal delta-ferrite (Fig. 2). To understand the cause for retention of delta-ferrite in the weld metal, DSC studies were performed.

### 3.2 Phase transformations

The DSC thermogram for P91B steel base metal during slow heating to melting temperature followed by slow cooling to room temperature is shown in Fig. 3 in which various phase transformations occurring during heating and cooling are indicated. The first thermal arrest occurs at a point where ferromagnetic to paramagnetic transformation of  $\alpha$ -ferrite takes place at the Curie temperature ( $T_c$ ) of  $748 \text{ }^\circ\text{C}$ . The microstructure of P91B steel consists of tempered martensite ( $\alpha'$ ) +  $M_{23}C_6$  + MX carbides/nitrides/carbonitrides. The temperature at which  $\alpha \rightarrow \gamma$  transformation starts is  $862 \text{ }^\circ\text{C}$  (at  $3 \text{ }^\circ\text{C min}^{-1}$  heating rate). Transformation from  $\alpha$  + carbide mixture occurs as  $\alpha + MX + M_{23}C_6 \rightarrow \alpha + \gamma + MX + M_{23}C_6$ , with  $M_{23}C_6$  precipitates starting to dissolve gradually with increase in temperature. This phase transformation continues over a temperature range, with starting temperature commonly referred to as  $A_{c1}$  and the finishing temperature as  $A_{c3}$ , and the phase field between these two critical temperatures is known as the inter-critical zone.

**Table 1** Chemical composition (in wt.%) of P91B steel

C	Cr	Mo	Si	Mn	V	Nb	S	P	Ni	Al	Ti	N	B	Cu	Fe
0.1	8.5	1.04	0.4	0.3	0.09	0.023	0.002	0.005	0.02	0.03	0.03	0.002	0.01	.003	Bal.

**Table 2** Electron beam welding parameters used

Weld ID	Accelerating voltage (kV)	Beam current (mA)	Focal length (mm)	Welding speed (mm min <sup>-1</sup> )	Heat input (J mm <sup>-1</sup> )
W1	120	60	355	600	720
W2	125	60	355	400	1125
W3	125	48.6	355	300	1212

Transformation above  $A_{c3}$  occurs as  $\alpha + \gamma + MX + M_{23}C_6 \rightarrow \gamma + MX + M_{23}C_6$ . The high temperature required for completion of this transformation is due to the sluggish kinetics of this phase transformation, which sometimes necessitates heating to  $\sim 50^\circ$  higher than  $A_{c3}$  during continuous

heating experiment to ensure completion of this austenitic phase transformation. The effect of heating associated with the residual part of this transformation is often much smaller than the heat of reaction of this transformation.

The presence of BN phase is also possible; however, its volume fraction is very low due to very low nitrogen in the material. Austenite formation is accompanied by dissolution of BN precipitates at 1123–1137 °C occurring as  $\gamma + MX + M_{23}C_6 + BN \rightarrow \gamma + MX + M_{23}C_6$ . In 9 Cr-0.5 Mo-1.8 W 0.2 V-0.05 Nb-0.005 B steel, complete dissolution of BN precipitates reported at the solutionising temperature of 1250 °C after 0.5 h of holding [7].

Delta-ferrite formation starts at 1235 °C occurring as  $\gamma + MX \rightarrow \delta + \gamma + M_{23}C_6$  and is followed by dissolution of MX precipitates. As volume fraction of MX precipitates is very

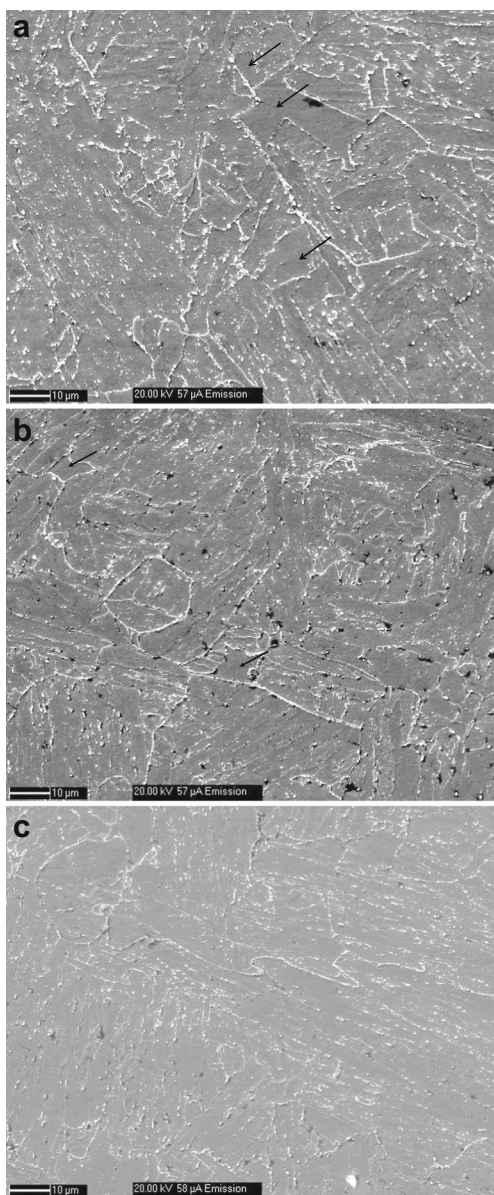


**Fig. 1** SEM micrographs of P91B steel EB weld metals after PWHT: a W1; b W2; c W3

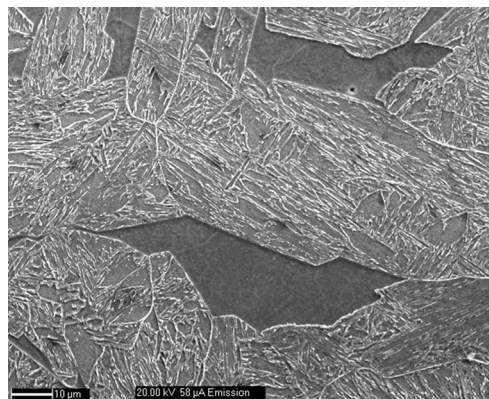


**Fig. 2** SEM micrograph of W1-P91B steel EB weld metal in as-welded condition

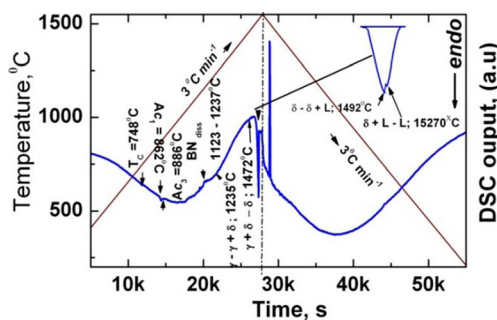


**Fig. 3** DSC thermogram illustrating the sequence of phase transformations occurring in P91B steel up to melting point under argon atmosphere

small (0.05 wt.% [8]), dissolution of MX is not accompanied by sharp thermal arrest. Delta-ferrite formation temperature depends on the balance between ferrite and austenite stabilizing elements, with transformation occurring as  $\delta + \gamma + \text{MX} \rightarrow \gamma + \delta$ , with  $\delta + \gamma$  being in equilibrium. Beyond this point, austenite slowly dissolves with increase in temperature, with the  $\delta + \gamma \rightarrow \delta$  transformation occurring as at 1472 °C, which is clearly marked by a sharp inflection point (Fig. 3). From this analysis, it is evident that delta-ferrite is present over a fairly large temperature range of 237 °C. This phase transformation is followed by the formation of liquid phase at 1492 °C, and melting occurs by peritectic reaction:  $\text{Liquid} + \delta \rightarrow \text{Liquid}$ .

During cooling cycle, transformation occurs in the reverse order, i.e., liquid solidifies as delta-ferrite first which then transforms to austenite. The transformation temperatures during cooling can be marginally different from those obtained during heating. However, high cooling rate which exist in weld metal may significantly influence the transformation temperatures. It was not possible to plug thermocouple in the weld pool as high vacuum system was used during EB welding. However, it is reasonable to assume that cooling rate can be controlled by preheating and welding speed which will have significant influence on delta-ferrite to austenite transformation kinetics. This explains why delta-ferrite was present observed in the P91B weld metal.

Room temperature stability of delta-ferrite in high-chromium steels can be estimated from empirical formulae, which include weighted effects of the ferrite and austenite forming elements, viz. chromium-equivalent ( $\text{Cr}_{\text{eq}}$ ) and nickel-equivalent ( $\text{Ni}_{\text{eq}}$ ), respectively, with the difference between  $\text{Cr}_{\text{eq}}$  and  $\text{Ni}_{\text{eq}}$  referred to as Ferrite Factor (FF). This aids in predicting the delta-ferrite content in the weld metal from its chemistry. Different formulae used to calculate  $\text{Cr}_{\text{eq}}$  and  $\text{Ni}_{\text{eq}}$  include the Schaeffler formula [9], where  $\text{Cr}_{\text{eq}} = \text{Cr} + 1.5 \text{ Si} + \text{Mo} + 5 \text{ V} + 0.5 \text{ Nb} + 0.75 \text{ W}$  and  $\text{Ni}_{\text{eq}} = \text{Ni} + 0.5 \text{ Mn} + 30 \text{ C} + 30 \text{ N} + 0.3 \text{ Cu} + \text{Co}$ . The Schaeffler formula was modified to improve the accuracy in predicting the microstructure. The more recent formulae increase the weighted effect of Mo and Si as ferrite-forming elements and include the Kaltenhauser formula [9] where  $\text{Cr}_{\text{eq}} = \text{Cr} + 6 \text{ Si} + 4 \text{ Mo} + 8 \text{ Ti} + 2 \text{ Al} + 4 \text{ Nb}$  and  $\text{Ni}_{\text{eq}} = 2 \text{ Mn} + 4 \text{ Ni} + 40 \text{ N} + 40 \text{ C}$  and Newhouse formula [9, 10] where  $\text{Cr}_{\text{eq}} = \text{Cr} + 6 \text{ Si} + 4 \text{ Mo} + 11 \text{ V} + 5 \text{ Nb} + 1.5 \text{ W} + 12 \text{ Al} + 8 \text{ Ti}$  and  $\text{Ni}_{\text{eq}} = 2 \text{ Mn} + 4 \text{ Ni} + 40 \text{ C} + 30 \text{ N} + 2 \text{ Co} + \text{Cu}$ . Table 3 lists the FF calculated using these formulae.

**Table 3** Calculated Ferrite Factor for P91B steel weld metal

Method	Schaeffler		Kaltenhauser		Newhouse	
	$\text{Cr}_{\text{eq}}$	$\text{Ni}_{\text{eq}}$	$\text{Cr}_{\text{eq}}$	$\text{Ni}_{\text{eq}}$	$\text{Cr}_{\text{eq}}$	$\text{Ni}_{\text{eq}}$
P91B steel	11.29	3.25	15.48	4.76	19.1	5.28
Ferrite Factor	8.04	10.72	13.82			

The Schaeffler diagram [9] suggests that the microstructure of P91B steel should be fully martensitic. However, the Kaltenhauser and Newhouse formulae suggest that the P91B weld metal may contain delta-ferrite at room temperature. It is to be noted that none of these formulas include the effect of cooling rate on the microstructure, and hence, the observed microstructure cannot be always fully explained by using these formulae. However, these formulae can be used to assess the propensity of high-chromium steel to stabilize the delta-ferrite in the weld metal.

### 3.3 Phase diagram

The results of ThermoCalc calculations for P91B steel is shown in Fig. 4. The Y-axis represents the phase fraction in linear scale from 0 to 1 whereas X-axis represents temperature in Celsius. From the figure, it is apparent that delta-ferrite is stable between 1220 and 1500 °C. Therefore, equilibrium stability of delta-ferrite is 280 °C which is close to that measured experimentally from DSC thermogram as shown in Fig. 3.

Therefore, the presence of delta-ferrite in the W1 and W2 welds is due to higher cooling rate that these welds experienced during cooling. From Fig. 4b, it is clear that MX type precipitate is low. This is due to lower nitrogen content (20 ppm) in P91B steel than that commonly used in P91 steel (0.065 wt.%). This will led to lower volume fraction of nitride and carbonitrides in P91 B steel. However, it is worth mentioning that creep strength of P91B steel is influenced by the presence of boron in  $\text{M}_{23}\text{C}_6$  precipitate which stabilize the microstructure by reducing coarsening rate of this precipitate and reducing the recovery of matrix microstructure [3, 4].

### 3.4 Charpy V-notch impact toughness

Figure 5 shows that the upper self-energy (USE) of P91B base metal is significantly higher than those of its EB weld metals. While toughness value of all weld metals is similar at room temperature, DBTT of the W3 weld metal (−44 °C) is lower than those of the W2 (−36 °C) and W1 (−27 °C) weld metals. This lower DBTT for W3 weld metal is attributed to the absence of delta-ferrite in the weld. The presence of delta-ferrite promotes formation of  $\text{M}_{23}\text{C}_6$  carbides at the delta-ferrite/matrix interface, and under dynamic loading conditions, these brittle precipitates act as source of easy crack initiation point thereby reducing welds toughness [11]. Figure 6 shows the presence of discontinuous  $\text{M}_{23}\text{C}_6$  precipitates at the delta-ferrite/matrix interface in W1 weld metal.

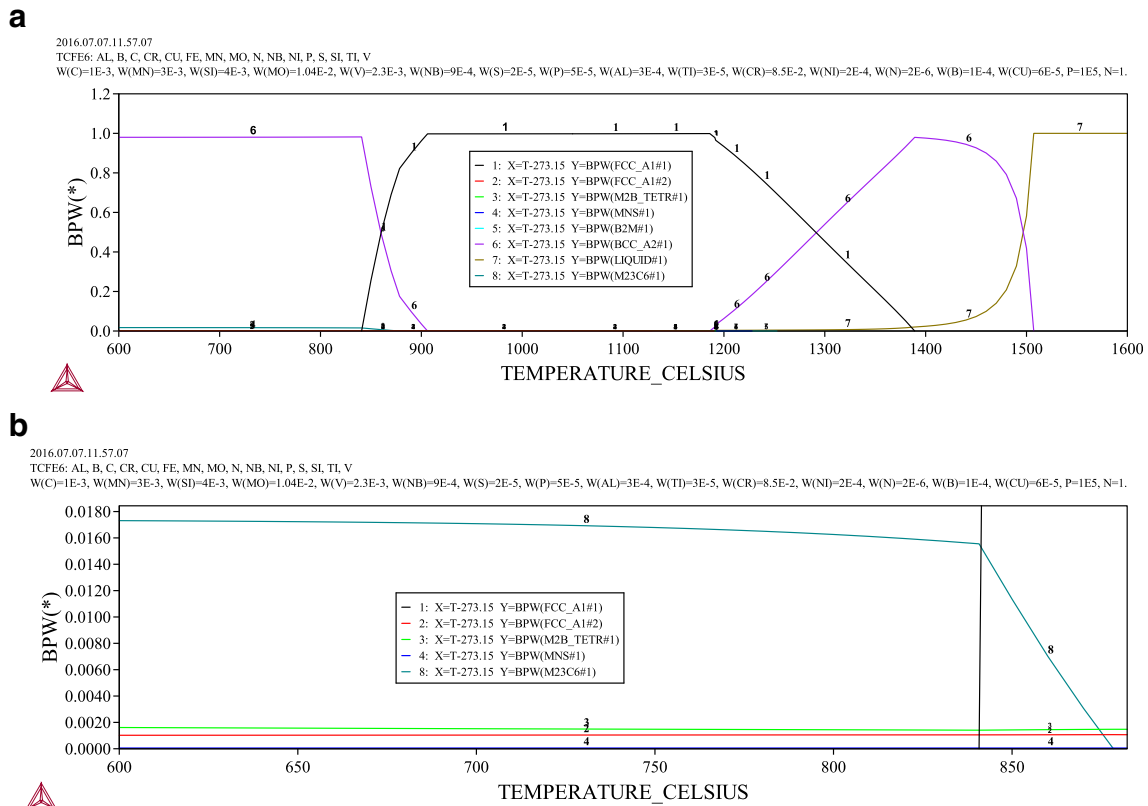


**Fig. 4** a Phase fraction diagram for P91B steel. b Phase fraction diagram for P91B steel, lower region

The fracture surface of W3 weld metal tested at room temperature (Fig. 7) shows ductile fracture. With decrease in test temperature, the fracture surfaces show quasi-cleavage and then cleavage fracture. At  $-40\text{ }^{\circ}\text{C}$ , the fracture surfaces show predominantly cleavage fracture in W1 weld metal (Fig. 8a), cleavage fracture with minute shear bands in W2 weld metal (Fig. 8b), and cleavage fracture with shear banding at the boundaries in W3 weld metal

(Fig. 8c), with the formation of shear bands indicative of the presence of a little ductility that contributes to lowering of DBTT. Arrow on Fig. 8a indicates the location of delta-ferrite. Thus, welding parameters, which affect retention of delta-ferrite, influence the DBTT of the EB welds. Therefore, it is necessary to control the cooling rate to achieve complete transformation of delta-ferrite to austenite in RAFM steel.

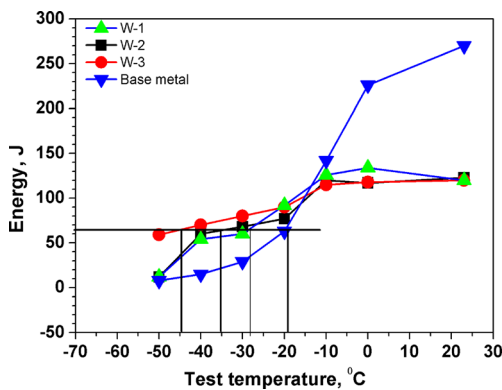


**Fig. 5** Variation in Charpy V-notch impact energy (average of two tests) with temperature for P91B steel EB welds (PWHT conditions)

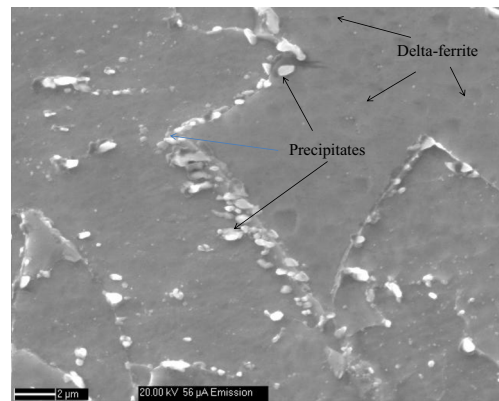


**Fig. 6** SEM micrograph showing precipitates at delta-ferrite/matrix interface in W1 weld metal

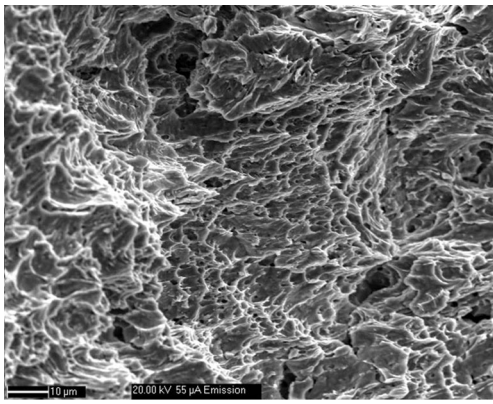


**Fig. 7** Fracture surface of W3 weld metal tested at room temperature

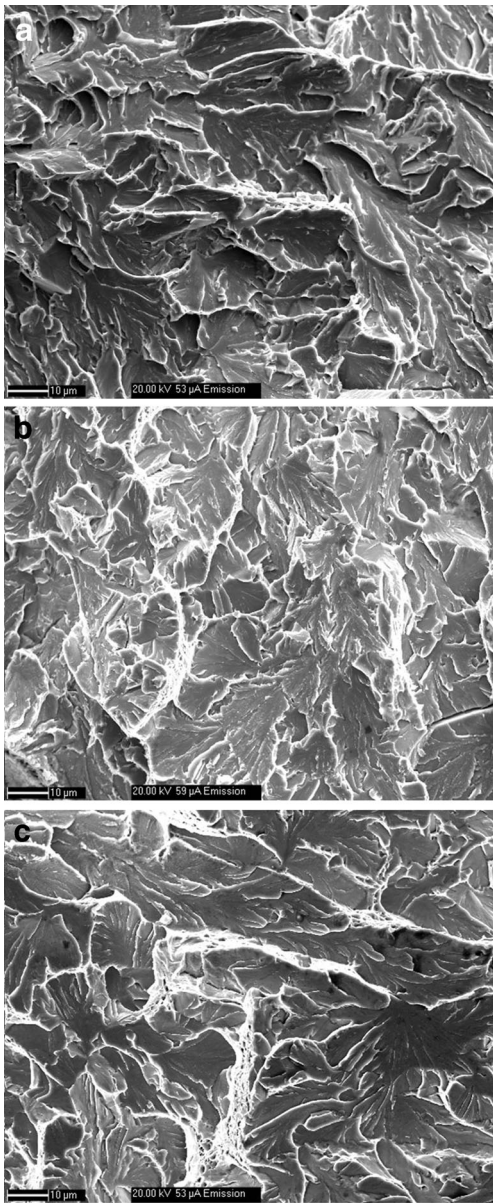


**Fig. 8** Fracture surfaces of **a** W1, **b** W2, and **c** W3 weld metals tested at  $-40\text{ }^{\circ}\text{C}$

## 4 Conclusions

The EB welding parameters significantly influences the delta-ferrite to austenite phase transformation. Relatively lower welding speed aids completion of the delta-ferrite to austenite phase transformation by providing more time for transformation. The reduced retention of delta-ferrite (as in the W3 weld metal) decreases the DBTT of the P91B steel EB weld metal. The upper-shelf energy of the P91B steel EB weld metal is lower than P91B base metal, and the DBTT of the EB weld metals is significantly lower than that of the P9B steel base metal.

**Acknowledgments** The support of Mrs. N. Sreevidya for SEM studies is gratefully acknowledged.

## References

1. Klueh RL and Harries DR (2001) High-chromium ferritic and martensitic steels for nuclear applications, American Society for Testing and Materials, West Conshohocken, Pa, USA
2. Ennis PJ, Czyrska-Filemonowicz A (2003) Recent advances in creep-resistant steels for power plant applications. *Sadhana* 28: 709–730
3. Das CR, Albert SK, Swaminathan J, Raju S, Bhaduri AK, Murty BS (2012) Transition of crack from type IV to type II resulting from improved utilisation of boron in the modified 9Cr-1Mo steel weldment. *Metall Mater Trans* 43A:3724–3741
4. Abe F, Tabuchi M, Kondo M, Tsukamoto S (2007) Suppression of type IV fracture and improvement of creep strength of 9Cr steel welded joints by boron addition. *Int J Press Vessel Pip* 84: 44–52
5. Mayr P (2007) Evolution of microstructure and mechanical properties of the heat affected zone in B-containing 9 % chromium steels. Ph. D. Thesis, University of Graz, Austria
6. Krishnamraju P (2014) Influence of weld chemistry and post weld heat treatment on micro structure and mechanical properties of P91 weld steels, M.Tech. Thesis, National Institute of Technology, Tiruchirapalli, India
7. Klueh RL (2008) *Reduced-activation steels: future development for improved creep strength*. *J Nucl Mater* 378:159–166
8. Yamada K, Igarashi M, Muneki S, Abe F (2002) Effect of heat treatment on precipitation kinetics in high-Cr ferritic steels. *ISIJ Int* 42:779–784
9. Onoro J (2006) *J Mater Process Technol* 180:137–142
10. Patriarca P et al. (1976) *Nucl Technol* 28:516–536
11. Divya M, Das CR, Mahadevan S, Albert SK, Pandian P, Kar SK, Bhaduri AK, Jayakumar T (2015) *Metall Mater Trans* 46A:2554–2567